Available online at www.sciencedirect.com
ScienceDirect
Polymer 47 (2006) 7198–7206
polymer
www.elsevier.com/locate/polymer

Molecular brushes as super-soft elastomers

Tadeusz Pakula [a,✠], Ying Zhang [a], Krzysztof Matyjaszewski [b,*], Hyung-il Lee [b], Hans Boerner [b], Shuhui Qin [b], Guy C. Berry [b]

[a] *Max-Planck Institute for Polymer Research, D55021 Mainz, Germany*
[b] *Department of Chemistry, Carnegie Mellon University, 4400 Fifth Avenue, Pittsburgh, PA 15213, USA*

Received 2 February 2006; received in revised form 1 May 2006; accepted 2 May 2006
Available online 30 June 2006

Dedicated to the memory of Tadeusz Pakula.

Abstract

Brush copolymers synthesized by controlled radical polymerizations were crosslinked either covalently or physically, resulting in elastomers with an unusually low equilibrium shear modulus G_e, of order 1 kPa. Examples are given for both crosslink motifs, along with the dynamic viscoelastic properties of these materials. The results are discussed in terms of the effect of the side chains on the brush polymers, which behave in some respect as a low molecular weight diluent that cannot be leached from the sample.

Keywords: Super-soft elastomers; Molecular brush; ATRP

1. Introduction

Developments in controlled radical polymerizations (CRPs) have opened the opportunity to create molecular structures devised to exhibit special properties [1]. Atom transfer radical polymerization (ATRP) and reversible addition-fragmentation transfer (RAFT) polymerization methods [2,3] have been applied to the synthesis of molecular brushes, i.e., densely grafted (or branched) copolymers. Molecular brushes can be prepared either by polymerization of a macromonomer already containing the chain that will become the branch (or a side chain), or by grafting the side chain from (or onto) a prepared linear chain. In either case, CRP permits control of the chain lengths of the backbone and side chains as well as their length distributions [1,4–6]. Either ATRP or RAFT were utilized to prepare backbones for molecular brushes and ATRP was employed for the subsequent grafting process to form densely branched brush-shaped polymer chains [7,8]. Furthermore, ATRP was used to prepare linear $-(B-A)_2$ and star-shaped $-(B-A)_3$ block copolymers, with a brush-shaped polymer as the central B segment, capped by outer A segments consisting of a polymer that is immiscible with the brush-shaped segment if both have a sufficiently high chain length [9–11]. The objective was to prepare and study soft materials that exhibit the behavior of a solid, with a very low equilibrium shear modulus G_e (or high equilibrium shear compliance $J_e = 1/G_e$). A brush polymer example of this type prepared by the polymerization of a macromonomer yielded a structure with G_e about 10-fold larger than the modulus described in this study [12].

Polymeric elastomers exhibiting solid-like behavior, formed via crosslink loci formed either by covalent bonds or physical aggregates stable under use conditions, are well known materials [13–15]. By contrast, for a polymeric fluid, $G_e = 0$, the material exhibits a steady-state recoverable shear compliance J_s. These features are represented in the well known linear viscoelastic expressions for the shear modulus $G(t)$ and the shear compliance $J(t)$ which are, of course, related to each other by a convolution integral [13–15]:

* Corresponding author.
E-mail address: km3b@andrew.cmu.edu (K. Matyjaszewski).
✠ Deceased 7 June, 2005.

0032-3861/$ - see front matter © 2006 Elsevier Ltd. All rights reserved.
doi:10.1016/j.polymer.2006.05.064

$$J(t) = R(t) + t/\eta \quad (1)$$

$$R(t) = J_\infty - (J_\infty - J_0)\, r(t) \quad (2)$$

$$G(t) = G_\infty + (G_0 - G_\infty)\, g(t) \quad (3)$$

where $R(t)$ is the recoverable shear compliance, $G_0 = 1/J_0$ is the so-called glassy modulus (reciprocal glassy compliance), observed at very short times at all temperatures, and even after a long time for T below the glass temperature T_g, G_∞ is G_e for a solid, or zero for a fluid, J_∞ is J_e for a solid and J_s for a fluid, and the reciprocal viscosity $1/\eta$ is zero for a solid, and greater than zero for a fluid. Both $g(t)$ and $r(t)$ decrease monotonically from unity to zero with increasing t, and are related to each other via the convolution integral of linear viscoelasticity. As a consequence of this behavior, $R(t)$ increases from J_0 for $t = 0$ to limiting values at large t of either to J_s for a fluid, or J_e for a solid. Although the contribution due to viscous deformation for a fluid appears explicitly in the term t/η in $J(t)$, the contribution is implicit in the representation for $G(t)$, being given by the integral of $G(t)$ over all t. A bilogarithmic plot of $R(t)$ vs. t may show an intermediate plateau with $R(t) \approx J_{ent}$ over a range of t if the molecular weight M is above a certain level M_{ent} for the undiluted polymer with density ρ; $M_{ent} = \rho RTJ_{ent}$ is the (average) molecular weight of the chain between entanglement constraints. With M much larger than M_{ent}, both J_{ent} and J are independent of M, but dependent on the polymer concentration c (wt/vol) if a diluent is present; to first-order, both are inversely proportional to c^2 [13–17]. Owing to the similarity of this behavior at intermediate t to the equilibrium behavior for a solid, J_{ent} is often called the "rubbery", "entanglement" or "(pseudo) network" plateau. Similarly, although it is frequently less pronounced unless M is very much larger than M_{ent}, bilogarithmic plots of $G(t)$ vs. t may exhibit a plateau for (the same) intermediate range of t, with $G(t)$ ca. $G_{ent} = 1/J_{ent}$. Although M_{ent} varies with chain structure, it often is in the range of 10 kDa [16].

Theoretical analysis of the dependence of G_e on molecular parameters leads to the following (somewhat simplified) expression in terms of the effective number density ν_{eff} of crosslink loci per unit volume, and G_{ent}:

$$G_e = \nu_{eff} kT + T_{ent} G_{ent} \quad (4)$$

where the fraction T_{ent} of "trapped" entanglements contributing to G_e may vary from zero to unity, depending on the preparation of the crosslinked network, among other factors [16,18]. For example, the crosslinking motifs shown schematically in Fig. 1 could lead to very different values of T_{ent}. The structure shown schematically in Fig. 1C is likely to lead to small T_{ent} if carried out in the presence of a diluent, and those in Fig. 1A and B could lead to large T_{ent} if carried out in the absence of a diluent.

To first-order, with neglect of "dangling chains" and certain other effects, for an undiluted polymer [15,16,18]

$$\nu_{eff} = \rho N_A / M_{xl} \quad (5)$$

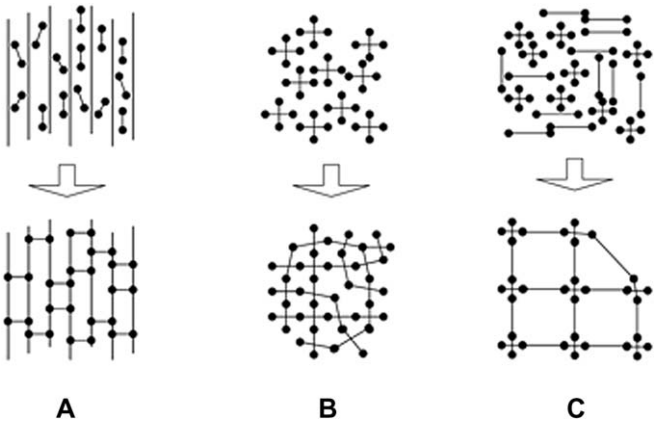

Fig. 1. Various ways to form polymer networks: (A) cross-linking of linear polymers (vulcanization), (B) polymerization of multifunctional monomers, and (C) linking of polymer ends by means of a cross-linking agent.

where M_{xl} is the average molecular weight of the chain between crosslink loci and N_A is the Avogadro's number. Since $G_{ent} = \rho RT/M_{ent}$ for the undiluted polymer, it can be seen that any contribution of trapped entanglements will act to place a lower bound of $\approx T_{ent} G_{ent}$ if $M_{xl} \gg M_{ent}$, unless T_{ent} is very small. This tends to place a lower bound of ≈ 100 kPa on the value of G_e that may be obtained in the undiluted crosslinked polymer. Smaller values may, of course, be obtained by the addition of diluent during crosslinking a preformed linear chain, as in Fig. 1C, taking advantage of the strong dependence of both ν_{eff} and G_{ent} on concentration (i.e., approximately c^{-2} as noted above).

The thrust of this study is to demonstrate means to obtain an undiluted crosslinked polymer with G_e much smaller than the values cited in the preceding paragraph. In essence, this is accomplished by crosslinking a brush-shaped polymer, characterized by a structure with relatively short branches (with molecular weight $M_{sc} \ll M_{ent,sc}$) placed on every repeat unit of a long backbone chain (with molecular weight $M_{bb} \gg M_{ent,bb}$). Some preliminary results on this methodology have been described in patent [19] or preprint form [20]. Similar observations on the effects of the side chains on G_{ent} for brush polymers have been presented to interpret data on a series of brush-shaped polystyrenes [21].

2. Experimental

2.1. Polymer synthesis

The preparation of various molecular brushes using the ATRP process is illustrated in Scheme 1, with $x = 1$, 2 or 3. The first polymerization step resulted in poly(2-(trimethylsilyloxy)ethyl methacrylate), poly(HEMA-TMS), **1** [22] with a topology dependent on the structure of the initiator. The ATRP process was used in all cases except for one, in which **1** was prepared by a RAFT process to provide a linear backbone with a very high degree of polymerization ($DP_n \approx 3500$), following prior methodology for both the ATRP and RAFT processes [23]. The linear poly(*n*-butyl acrylate), poly*n*BuA, sample was prepared by ATRP. All monomers, catalysts and

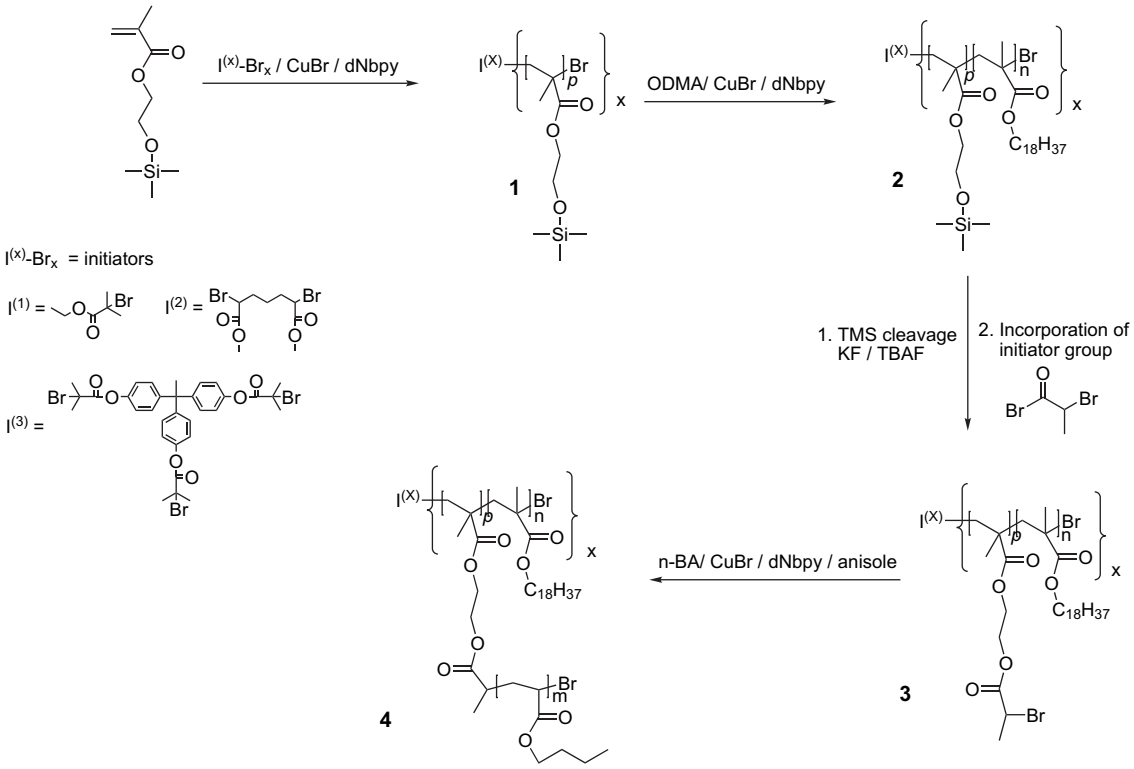

Scheme 1.

solvents were prepared and purified as described previously [22,24].

As illustrated in Scheme 1, 2-(trimethylsilyloxy)ethyl methacrylate (HEMA-TMS) was polymerized to yield poly(HEMA-TMS), **1**, the precursor for all of the brush structures [25]. In this scheme, $I^{(x)}$ represents the initiator fragment retained in the chain. Ethyl 2-bromoisobutyrate was used as the initiator for $x = 1$, with chain growth in one direction, dimethyl 2,6-dibromoheptanedioate was the initiator for $x = 2$, with chain growth in two directions and 1,1,1-tris(4-(2-bromoisobutyryloxy)phenyl)ethane was the initiator for $x = 3$ with chain growth in three directions, to yield three-arm star-shaped macromolecules. The Br end groups in **1** were optionally extended with poly(octadecyl methacrylate), poly(ODMA), segments forming $I^{(1)}$-B–A, $I^{(2)}$-(B–A)$_2$ and $I^{(3)}$-(B–A)$_3$ block copolymers, **2**. The TMS groups in **2** were replaced by 2-bromopropionate groups, capable of initiating ATRP of side chains, forming the brush precursor, **3**. In the final step, side chains were grown to the desired length to form brush block copolymers, **4**. A sample of poly(BPEM$_p$-*graft*-poly(*n*BuA$_m$)) was partially crosslinked by heating in the presence of a residual copper catalyst.

The degrees of polymerization p, m and n given in Table 1 for the resulting polymers were calculated from the monomer conversion assuming quantitative initiation. In prior work on similar poly(BPEM$_p$-*graft*-poly(*n*BuA$_m$)), it was found that M_n determined in this way was in good agreement with the value determined through the use of a light scattering detector on an SEC column [26]. The entries for M_w/M_n given in Table 1 are estimated from an SEC analysis based on a molecular weight calibration for the SEC columns with linear poly(methyl methacrylate) standards. Although the estimates in M_w and M_n are expected to be in error, principally owing to the neglect of the difference in molar mass of the repeating unit of the analyte polymer and that used in the calibration, the error is expected to be much smaller for M_w/M_n, becoming negligibly small with decreasing difference in the values of the Mark–Houwink–Sakarada exponent $\mu = \partial \ln[\eta]/\partial \ln M$ for the analyte and standard [27]. Accordingly, values of M_w/M_n for some brush molecules determined via an SEC analysis with standard molecular weight calibration were found to be similar to values deduced from a visualization of the polydispersity based on AFM analysis [28]. An NMR analysis used to determine the content of the ODMA and BuA fragments, yielded results consistent with the values expected from the monomer conversion.

Table 1
Characterization data for the samples used in this study

Sample[a]	f (wt% ODMA)	$M_{n,kin}$[b]	M_w/M_n[c]
p(*n*BuA)$_{480}$	0	61,000	1.15
p(BPEM$_{3500}$-*g*-p(*n*BuA)$_{30}$)	0	14,300,000	1.38
Crosslinked p(BPEM$_{400}$-*g*-p(*n*BuA)$_{30}$)	0	–	–
-(-p(BPEM$_{117}$-*g*-p(*n*BuA$_{46}$)-*b*-pODMA$_{205}$)$_2$	8.8	1,580,000	1.32
-(-p(BPEM$_{300}$-*g*-p(*n*BuA$_{35}$)-*b*-pODMA$_{20}$)$_3$	0.47	4,270,000	1.38
-(-p(BPEM$_{300}$-*g*-p(*n*BuA$_{35}$)-*b*-pODMA$_{360}$)$_3$	7.9	4,640,000	1.78

[a] p = poly, *g* = graft, *b* = block; see the text for additional abbreviations.
[b] Based on the monomer conversion and the initiator concentration, as discussed in the text.
[c] Based on SEC analysis via a linear poly(methyl methacrylate) standard, as discussed in the text.

2.2. Mechanical properties

Dynamic mechanical measurements were performed using the Rheometrics RMS 800 mechanical spectrometer, using parallel plates (6 mm diameter and 1 mm plate separation), under dry nitrogen atmosphere following methods described elsewhere [29]. Shear deformation was applied under condition of controlled deformation amplitude, always remaining in the range of the linear viscoelastic response of studied samples. The data, measured over the frequency range 0.1–100 rad/s at various temperatures, were expressed as the dynamic storage and loss shear moduli, $G'(\omega)$ and $G''(\omega)$, respectively. The data on $G'(\omega)$ and $G''(\omega)$ vs. ω at the several temperatures measured were superposed to form a ''master'' graph of $G'(a_T\omega)$ and $G''(a_T\omega)$ vs. $a_T\omega$ (i.e., only shifts of $\log[G'(\omega)]$ and $\log[G''(\omega)]$ along $\log(\omega)$ were performed, using a reference temperature $T_{ref} = 254$ K. For certain samples, the well known formulae of linear viscoelasticity [13,15] were used to compute the dynamic storage and loss shear compliances $J'(a_T\omega)$ and $J''(a_T\omega)$, respectively, as functions of $a_T\omega$ from the reduced dynamic moduli, using a selection of evenly spaced points along the bilogarithmic curves of the superposed dynamic moduli. Independently, the isochronal temperature dependence of these $G'(\omega)$ and $G''(\omega)$ was determined for $\omega = 10$ rad/s.

2.3. Small-angle X-ray scattering

The apparatus and methods described elsewhere [30] were used to acquire small-angle X-ray (SAXS) data on two samples as described below. The scattering with 0.154 nm wavelength incident radiation wavelength collected with a 2D detector is presented below as a function of the modulus q.

3. Results and discussion

3.1. The brush copolymer

The data on $G'(a_T\omega)$, $G''(a_T\omega)$ and $\tan[\delta(a_T\omega)] = G''(a_T\omega)/G'(a_T\omega)$ as functions of the reduced frequency $a_T\omega$ in Fig. 2 for the linear poly(nBuA), with $M_n = 61.5$ kDa prepared in this study, along with data scanned from the literature [31] for a sample with $M_n = 362$ kDa, are shown for comparison with the properties of a linear brush chain, with short poly(nBuA) side chains to illustrate an evaluation of G_{ent} for poly(nBuA). These data are analyzed by a method used in the literature which evaluates G_{ent} as the value of $G'(\omega_{min})$, where ω_{min} is the frequency for a minimum in $\tan\delta = G''(\omega)/G'(\omega)$. The estimates for the two molecular weights differ slightly, with the data on the higher molecular weight sample giving $G_{ent} \approx 0.12$ MPa. The anticipated behavior for a viscoelastic fluid with $G'(\omega) \propto \omega^2$ and $G''(\omega) \propto \omega$ is seen in the limit of low ω. The same data recast as $J'(a_T\omega)$ and $J''(a_T\omega)$ as functions of $a_T\omega$ are given in Fig. 3 for comparison. The representations in terms of the dynamic moduli and compliances

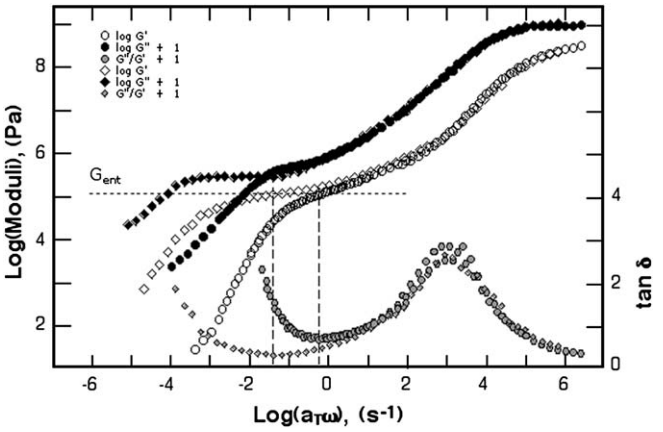

Fig. 2. Plots of $\log G'(a_T\omega)$, $\log G''(a_T\omega)$ and $\tan\delta$ vs. the reduced frequency $\log a_T\omega$ for melts of linear poly(nBuA) with $M_n = 61.5$ kDa (circles) and 320 kDa (diamonds) calculated from data in the literature [31]. The lower curve gives $\tan\delta$, and for the upper curves, the unfilled and filled symbols correspond to $G'(\omega)$ and $G''(\omega)$, respectively. The dashed horizontal line indicates the level of the entanglement plateau G_{ent}, estimated by a method which evaluates G_{ent} as the value of $G'(\omega_{min})$, where ω_{min} is the frequency for a minimum in $\tan\delta(\omega) = G''(\omega)/G'(\omega)$. The data tend to the limiting behavior $G'(\omega) \propto \omega^2$ and $G''(\omega) \propto \omega$ expected for any viscoelastic fluid with decreasing ω.

emphasize aspects of $J(t)$ and $G(t)$ given in Eqs. (1) and (3), respectively. Thus, for a linear viscoelastic material:

$$J'(\omega) - J_0 = (J_\infty - J_0)\left\{1 - \omega\int_0^\infty du\, r(u)\sin(\omega u)\right\} \quad (6)$$

$$J''(\omega) - 1/\omega\eta = (J_\infty - J_0)\omega\int_0^\infty du\, r(u)\cos(\omega u) \quad (7)$$

$$G'(\omega) - G_\infty = (G_0 - G_\infty)\omega\int_0^\infty du\, g(u)\sin(\omega u) \quad (8)$$

$$G''(\omega) = (G_0 - G_\infty)\omega\int_0^\infty du\, g(u)\cos(\omega u) \quad (9)$$

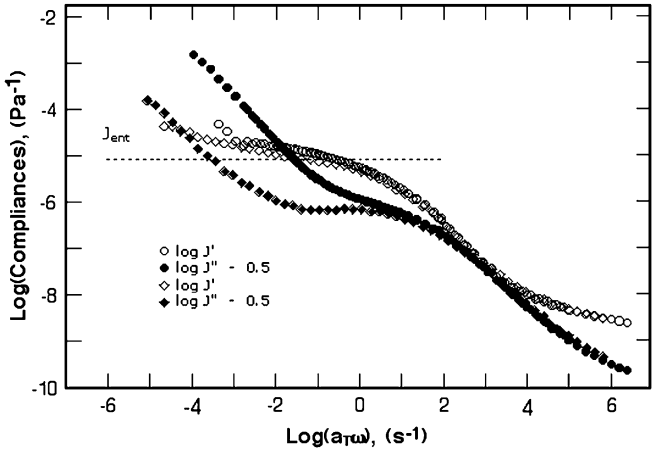

Fig. 3. Bilogarithmic plots of $J'(a_T\omega)$ and $J''(a_T\omega)$ vs. the reduced frequency $a_T\omega$ for melts of linear poly(nBuA) for the data in Fig. 2, using the same symbol convention. The dashed horizontal line indicates the level of the entanglement plateau J_{ent}. With decreasing ω, the data tend to the limiting behavior with $J''(\omega) \propto \omega^{-1}$ and $J'(\omega) \propto$ constant expected for any viscoelastic fluid in the limit of low ω.

Consequently, whereas the contribution from viscous deformation for a fluid appears implicitly in the integrals in both $G'(\omega)$ and $G''(\omega)$, the same contribution appears as a separable term in the expression for $J''(\omega)$, and is not involved at all in $J'(\omega)$. This feature can be especially useful in examining the behavior with ω near or less than the value in the regime with the intermediate plateau in $J'(\omega)$, and will be employed throughout to gain that advantage. The results for the higher molecular weight sample show a plateau in $J'(\omega)$ that gives $J_{ent} \approx 7.8\ \mu Pa^{-1}$ ($G_{ent} \approx 0.13$ MPa) in $J'(\omega)$ at intermediate frequency and an approach at low frequency that approximates $J_s \approx 40.7\ \mu Pa^{-1}$. The anticipated behavior for a viscoelastic fluid with $J''(\omega) \propto \omega^{-1}$ is seen in the limit of low ω. The data on the lower molecular weight sample do not show a clear separation of these two modes, reflecting the lower entanglement density in that polymer. The ratio $J_s/J_{ent} \approx 5.2$ is larger than the value $J_s/J_{ent} \approx 3$ that is normal for a linear flexible chain with a narrow molecular weight distribution, [13,14] possibly indicating that the higher molecular weight sample is mildly polydisperse in M. The estimates of G_{ent} given above correspond to $M_{ent} \approx 17$ kDa, showing that the $M_{sc} \ll M_{ent}$ for the polymer used here (the same conclusion would be reached using a higher estimate of M_{ent} available in the literature, apparently without the benefit of data in the literature that may be evaluated) [32].

The results on $G'(a_T\omega)$ and $G''(a_T\omega)$ for the poly(BPEM-*graft*-poly(*n*BuA)) brush polymer, and the crosslinked brush are shown in Fig. 4, with the behavior for $J'(a_T\omega)$ and $J''(a_T\omega)$ for the same samples given in Fig. 5. Although the entanglement plateau is not well defined prior to crosslinking, the use of the criterion above with $G_{ent} \approx G'(\omega_{min})$ gives $G_{ent} = 1/J_{ent} \approx 0.5$ kPa, which is a rather small value of G_{ent} for an undiluted polymer. Furthermore, $J'(\omega)$ continuing to increase with decreasing ω down to the lowest frequency accessible with the equipment in use, tending to a rather large, but inaccessible, value of J_s, indicating that the unseen J_s would give J_s/J_{ent} much larger than the value $J_s/J_{ent} \approx 3$ that is normal for a linear flexible chain with a narrow molecular weight distribution. By comparison, as shown in Figs. 4 and 5, $G_e = 1/J_e \approx 1.6$ kPa, for G_{ent} is too small, or that $M_{xl} < M_{ent}$, so that the first term in Eq. (10) controls the value of G_e for the crosslinked brush polymer studied here. Similar results with a somewhat higher $G_e \approx 10$ kPa have been reported for a brush polymer prepared by polymerization of a poly(ethylene oxide) methacrylate macromonomer [12], as opposed to the modification of a preexisting linear polymer adopted in this study.

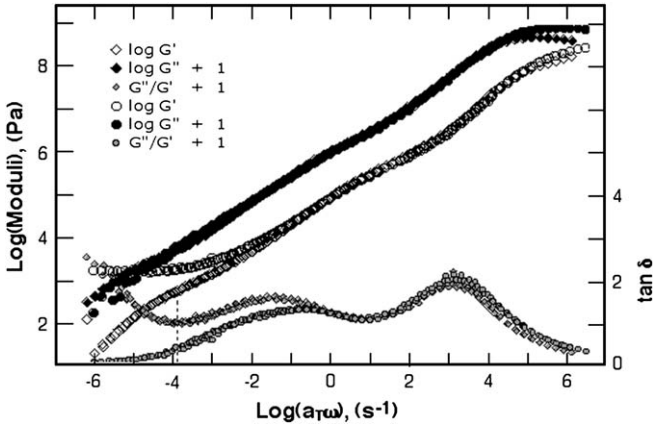

Fig. 4. Plots of log $G'(a_T\omega)$, log $G''(a_T\omega)$ and tan δ vs. the reduced frequency log $a_T\omega$ for a melt of linear melt of poly(BPEM-*graft*-poly(*n*BuA)) molecular brushes with $DP_{bb} = 3500$ monomer units and $DP_{sc} = 30$ (diamonds) and the crosslinked brush polymer (circles). The lower curve gives tan δ, and for the upper curves, the unfilled and filled symbols correspond to $G'(\omega)$ and $G''(\omega)$, respectively. The dashed vertical line indicates the frequency ω_{min} for a minimum in tan $\delta(\omega) = G''(\omega)/G'(\omega)$ used to estimate G_{ent} as the value of $G'(\omega_{min})$.

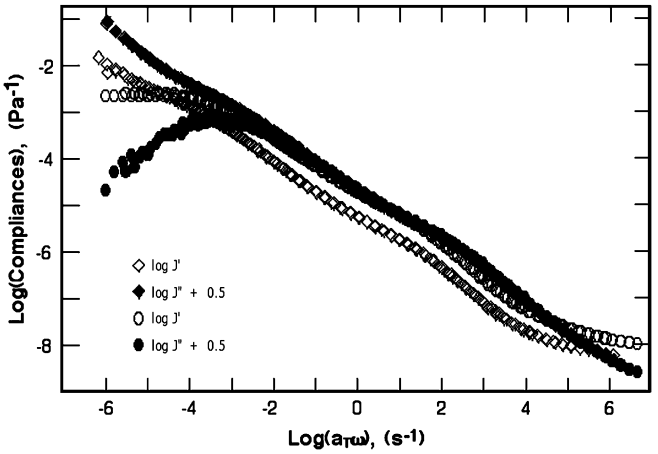

Fig. 5. Bilogarithmic plots of $J'(a_T\omega)$ and $J''(a_T\omega)$ vs. the reduced frequency $a_T\omega$ corresponding to the data shown in Fig. 4. The plateau in $J'(a_T\omega)$ for the crosslinked sample is the level of J_e, and it may be seen that whereas $J''(a_T\omega)$ tends to proportionality with $(a_T\omega)^{-1}$ for low ω for the uncrosslinked sample, as expected for a fluid (e.g., see Fig. 3), for the crosslinked sample $J''(\omega)$ tends toward small values in the same limit, as expected for a solid.

The temperature dependence of $G'(\omega)$ and $G''(\omega)$ is shown in Fig. 6 at a fixed frequency, $\omega = 1$ rad/s. As would be anticipated, G_e given by the value of $G'(\omega)$ for $T \approx T_g + 100$ is nearly independent of T.

This rather large J_{ent} given above for the uncrosslinked brush polymer, or correspondingly small $G_{ent} = 1/J_{ent}$, is attributed to the copious branching in the brush polymer. The enhanced

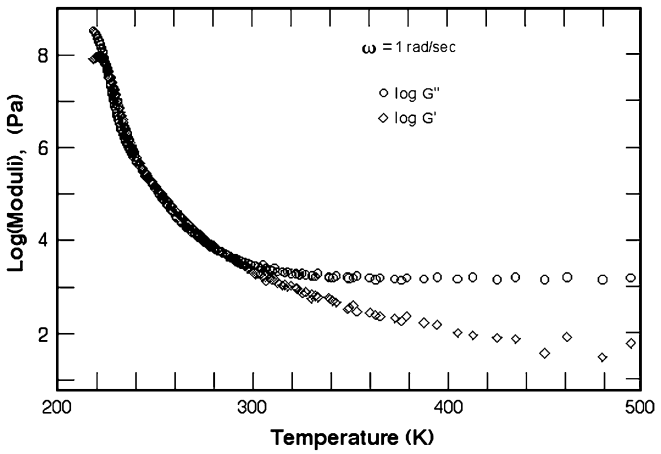

Fig. 6. Plots of the logarithm of $G'(a_T\omega)$ and $G''(a_T\omega)$ vs. temperature for the crosslinked sample in Fig. 4, showing that G_e tends to be independent of temperature for T well above the glass temperature T_g.

J_s/J_{ent} is attributed to a dispersity of relaxations of chain segments traced from the end of one branch through the backbone to the end of a second branch. Similar, though much weaker behavior may be seen in Fig. 7, prepared from data reported for comb-shaped polystyrenes with branches much shorter than the backbone, and with $M_{bb} \gg M_{ent,bb}$ and $M_{sc} \ll M_{ent,sc}$, where M_{ent} is the entanglement molecular weight of the undiluted linear polymer, similar to the situation encountered in this work [33]. The effects on J_{ent} and J_s for the comb-branched polymer were interpreted in an approximate way by treating the branches as a diluent in calculating estimates for these quantities. Thus, in that work, J_s for the entangled polymer was interpreted by the expression normally used for a flexible linear chain present at concentration c, with c and M replaced by the concentration $c_{bb} = \rho M_{bb}/(M_{bb} + pM_{sc})$ and molecular weight M_{bb} of the backbone, respectively, to give [33]

$$J_s \propto \frac{\rho M_{ent}}{c_{bb}^2 RT} \tag{10}$$

For the data in Fig. 7, the values of $J_{ent} \approx J'(\omega)$ for ω in the range for the plateau J_{ent} for the linear polymer give J_{ent}/J_s that decreases with increasing M_{sc}; in fact, for these data, $J_{ent} \approx \rho M_{ent}/c_{bb}RT$, e.g., $J_{ent} = 1/G_{ent}$, with G_{ent} calculated using the expression given above, with ρ replaced by c_{bb}. It may be observed that the distinction in the behavior in the intermediate frequency range is not as evident in representations of the data in terms of $G'(\omega)$ and $G''(\omega)$. Similar behavior has been reported for binary blends of linear polystyrenes, with components having molecular weights $M_{low} < M_{ent}$, and $M_{high} \gg M_{ent}$ [34,35]. The results gave $J_{ent}/J_s \approx 1$, different from the behavior noted for the comb-branched polymer, but J_s could be fitted by Eq. (10) with c_{bb} taken to be the concentration of the high molecular weight component. A more complete analysis of the effects of branches on the viscoelastic properties has been presented on the basis of the so-called tube dilation models, principally to understand the effects of branches with $M_{sc} > M_{ent}$ [36] and that model has been applied to such data given in Ref. [33] on additional comb-branched polystyrenes.

In the application of Eq. (10) to the data on the materials in this study, $c_{bb} = \rho M_{bb}/(M_{bb} + pM_{sc})$, with the number of branches $p = DP_{bb}$ so $c_{bb} \approx \rho/DP_{sc} \approx \rho/30$. Thus, one might expect an enhancement in J_s of about 30^2 over what would be observed for the polymer without the branches. Similarly, replacement of ρ by c_{bb} in the expression for G_{ent} would result in a suppression of G_{ent} by 30. For comparison, $G_{ent} \approx 0.30$ MPa for poly(methyl methacrylate), PMMA [16], and the data in Fig. 2 give $G_{ent} \approx 0.13$ MPa for poly(*n*BuA). Based on the data for PMMA, one might anticipate $G_{ent} \approx$ 4–9 kPa for the poly(BPEM-*graft*-poly(*n*BuA)) brush studied here, in the range reported above. Insofar as the modulus G_e depends on G_{ent} for the material prior to crosslinking, G_e for the crosslinked brush polymer is seen to depend on the branch length through the effect of the latter on c_{bb}. Owing to effects not included in this crude approximation, such as effects of the side chain length on the persistence length of the backbone, the actual behavior may be more complicated.

Inspection of Figs. 4 and 5 reveals some weak inflections in both the dynamic moduli and compliances for $a_T\omega$ in the range 1–3. It is possible that this may reflect the side chain dynamics, similar to the analysis described above comb-branched polymers [33]. One would, however, require data on brush polymers over a range of side chain molecular weight to assess this speculation.

The behavior of the crosslinked brush polymer in successive stress–strain cycles in tension at room temperature under successively increasing maximum strains ε_{max}, up to $\varepsilon_{max} = 1.2$, is shown in Fig. 8. The hysteresis in the stress–strain cycle reveals the viscoelastic character of the crosslinked polymer, as well as the very good reversibility of the material response up to a rather large tensile deformation.

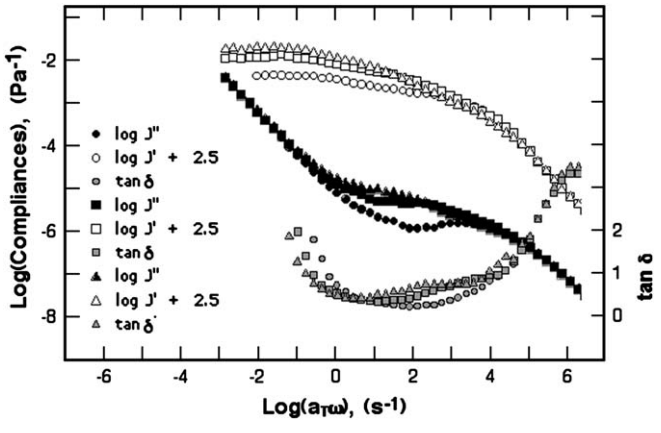

Fig. 7. Plots of $\log J'(a_T\omega)$, $\log J''(a_T\omega)$ and $\tan\delta(a_T\omega)$ vs. the reduced frequency $\log a_T\omega$ for a linear polystyrene ($M_w = 275$ kDa), circles and comb-branched molecules with branches attached to the same linear chain as the backbone: 31 branches with $M_w = 6.5$ kDa, squares, and 30 branches with $M_w = 11.7$ kDa, triangles. The lower curve gives $\tan\delta$, and for the upper curves, the unfilled and filled symbols correspond to $J'(\omega)$ and $J''(\omega)$, respectively. Calculated from $G'(\omega)$ and $G''(\omega)$ in Ref. [33].

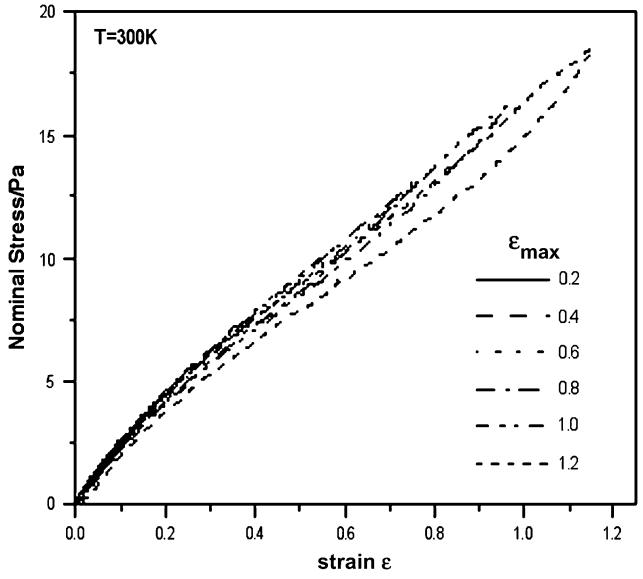

Fig. 8. The nominal tensile stress vs. the strain in tension for stress–strain cycles with successively larger maximum strains for the crosslinked brush polymer.

3.2. Phase-separated block copolymers

A study of phase separation in -(-poly(BPEM$_{117}$-*graft*-poly(*n*BuA)$_{46}$-*block*-polyODMA$_{205}$)$_2$ triblock copolymers which established a phase diagram with several ordered phases [30] provides some insight on the phase behavior anticipated with the system in this study. Based on that work, the compositions studied here with 0.47 and 7.9 wt% of the poly(ODMA) component would be expected to be homogeneous and near the conditions for phase separation, respectively. A simplified schematic drawing of a network structure that could develop with the star-shaped polymer is shown in Fig. 9. In the actual case, the phase-separated domains will be more complex, with poly(ODMA) segments from more than a three molecules participating in a single phase-separated poly(ODMA) domain. Since premature termination can lead to structures without the poly(ODMA) block, the star-shaped geometry reduces the probability that for the formation of a chain with only a single poly(ODMA) block in comparison with the double-ended molecule derived from a difunctional initiator.

The data on $J'(a_T\omega)$ and $J''(a_T\omega)$ in Fig. 10 are for star-shaped polymers -(-poly(BPEM$_{300}$-*graft*-poly(*n*BuA)$_{35}$-*block*-polyODMA$_n$)$_3$, with $n=20$, $f=0.47$ wt% and $n=360$, $f=7.9$ wt%, and those in Fig. 11 are for the ''linear'' homolog -(-poly(BPEM$_{117}$-*graft*-poly(*n*BuA)$_{46}$)-*block*-polyODMA)$_{205}$)$_2$ with $f=8.8$ wt%. The data on the two materials with the larger weight fraction f of the ODMA component exhibit behavior consistent with a phase-separated system, showing a plateau in $J'(a_T\omega)$ at low frequency. The data for the star-shaped sample with $f=0.47$ wt% exhibit no such plateau, indicating fluid behavior similar to that reported above for the brush polymer prior to crosslinking. The plateau for the star-shaped sample with $f=7.9$ wt% displays what appears to be an equilibrium compliance given by $G'_{\text{plateau}}=1/J'_{\text{plateau}}\approx 0.65$ kPa, while the data in Fig. 11 give the estimate $G'_{\text{plateau}}\approx 1.35$ kPa at the lowest frequency, with a higher value, $G'_{\text{plateau}}\approx 6.1$ kPa apparent in the superposed data at higher frequency, marking a failure in the temperature–frequency superposition for this sample. This failure may reflect some crystallization of the poly(ODMA) blocks at the lower temperature used to access these higher reduced frequency data. These plateau values are about the same level as reported for J_{ent} in the preceding for the brush polymer, suggesting the same role for the side chains as discussed above for the covalently crosslinked brush polymer.

Ordered body centered cubic (bcc) phase-separated block copolymers are known to exhibit values of G'_{plateau} in this same range for intermediate frequency, resulting from fluctuations of the lattice formed by phase-separated blocks, with this plateau followed by fluid-like behavior with $G'(\omega)$ and $G''(\omega)$ tending toward proportionality with ω^2 and ω, respectively, for lower ω [37]. However, the small-angle X-ray scattering shown in

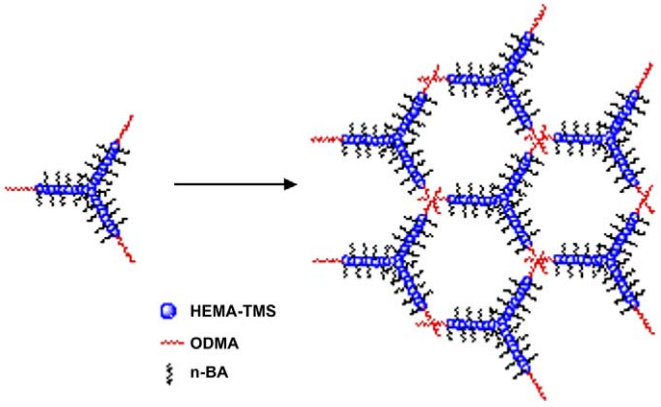

Fig. 9. A simplified schematic representation of the organization in the phase-separated sample of the star-shaped block copolymer, with the poly(ODMA) end blocks separated from the brush polymer interior chain sections. In actuality, in the 3D phase-separation, the poly(ODMA) domains would comprise chains from more than three of the star-shaped polymers.

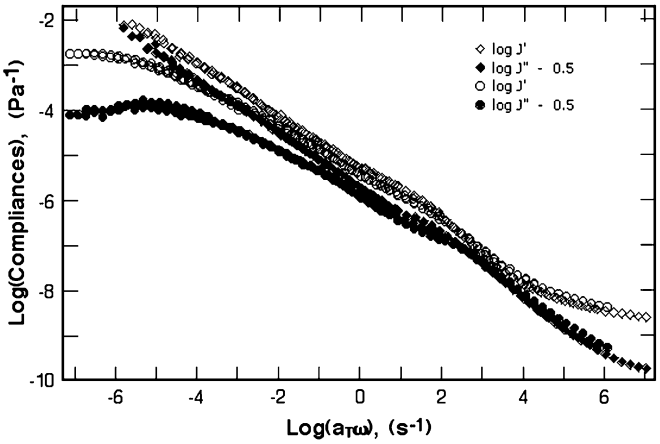

Fig. 10. Bilogarithmic plots of $J'(a_T\omega)$ and $J''(a_T\omega)$ vs. the reduced frequency $a_T\omega$ for two star-shaped block copolymers with weight fractions f of the poly(ODMA) blocks of 0.0047 (diamonds) and 0.079 (circles). A plateau in $J'(\omega)$ is seen for the latter physically crosslinked sample, and whereas $J''(\omega)$ tends to proportionality with ω^{-1} for low ω for the sample with $f=0.0047$, as expected for a fluid, the data for the sample with $f=0.079$ appear to exhibit a weak maximum at low ω followed by a tendency to increase slightly, suggesting the possibility that a fluid-like behavior could be observed at still lower frequency.

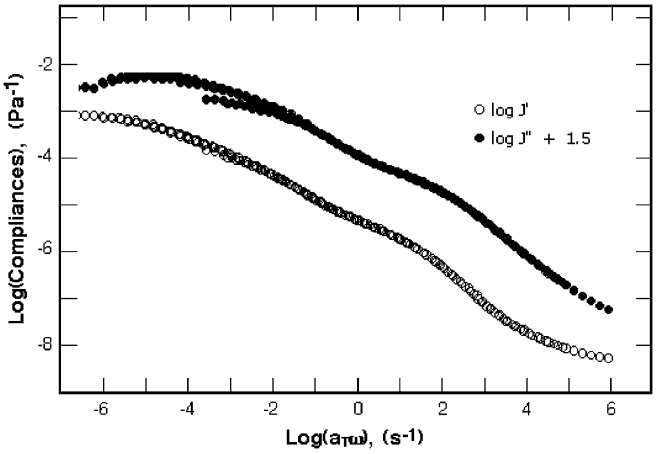

Fig. 11. Bilogarithmic plots of $J'(a_T\omega)$ and $J''(a_T\omega)$ vs. the reduced frequency $a_T\omega$ for a linear triblock copolymers with weight fractions $f=0.088$ of the poly(ODMA) blocks. The lack of complete frequency–temperature superposition may reflect crystallization of the poly(ODMA) domains. Calculated from $G'(a_T\omega)$ and $G''(a_T\omega)$ in Ref. [20].

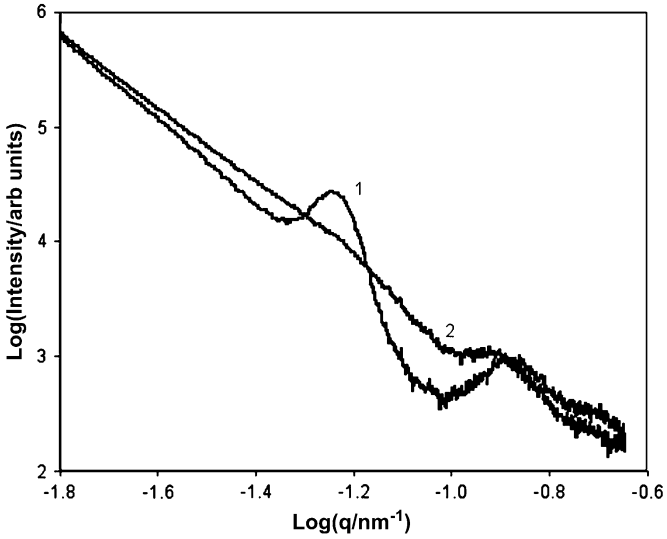

Fig. 12. The small-angle X-ray scattering observed for the two star-shaped block copolymers, with weight fractions $f = 0.0047$ (2) and 0.079 (1) of the poly(ODMA) blocks.

Fig. 12 does not indicate the presence of such a lattice with the polymer formed here. The positions $q_{\max,i}$ of the peaks at increasing q with respect to the first peak do not increase in the order expected for a bcc lattice, nor for the order expected for other often observed structures (hexagonal packing of cylinders, etc., as observed with the study on triblock copolymers cited above [30]), e.g., $q_{\max,1}/q_{\max,2} \approx 2.4$, and though $q_{\max,3}$ is not well defined, $q_{\max,1}/q_{\max,3} \approx 3.5$. These values suggest a rather disordered system, perhaps owing to the long time that would be required to form such a system. The range of temperatures at which the low-frequency plateau is observed for the sample with star-shaped molecules is well above the melting or glass transition temperatures for the components. It may be surprising, therefore that the data do not display the flow characteristic of a fluid (e.g., $J''(\omega) \propto \omega^{-1}$) at low frequency, in which case the plateau in $J'(\omega)$ mentioned above may not be a true equilibrium compliance, but rather an intermediate behavior obtained over a range of fairly low frequencies, with a level controlled by the entanglement density in the continuous domain of the brush polymer middle blocks. Indeed, there is some hint of an upswing of $J''(\omega)$ toward the behavior expected of a fluid at the lowest frequencies (and highest temperature) available for the data in both Figs. 10 and 11, suggestive of the onset of fluid-like behavior. One would, of course, anticipate that this fluid behavior would be eliminated if the phase-separated domains were either crystalline or glassy, e.g., as mentioned above the domains may have been crystalline for the lower temperatures (lower $a_T\omega$) for the data shown in Fig. 12.

4. Conclusion

The results described in this work show that a diluent-free melt polymer with a brush-like structure comprising relatively short side chains attached to every repeat unit of a backbone polymer can exhibit behavior that would normally be associated with the behavior of the backbone polymer without the side chains, but containing an equivalent concentration of a small molecule diluent. For the chain covalently crosslinked, this leads to an equilibrium modulus G_e that is unusually small for an undiluted melt polymer (e.g., $G_e \approx 1$ kPa for the sample studied here), more typical of a network swollen by a diluent. Furthermore, a material with a similarly low plateau modulus $G'_{plateau}$ over a range of frequencies similar to the observation of G_e for the covalently crosslinked polymer may be obtained with a triblock sample with a brush polymer middle section, and outer blocks immiscible with the brush polymer that phase separate into discrete domains. This plateau would correspond to an equilibrium modulus G_e if the domains can be fixed by going to a range of temperature for which they are either crystalline or glassy.

The viscoelastic solids with an equilibrium modulus in the range found here for systems based on brush polymer structures could find use in applications in which a low modulus is required, but it would be undesirable to have that level based on added diluent that might be leached from the composition over time. For examples, in biological applications which require a soft viscoelastic material that will not leach undesirable components into the surrounding tissue, electronic applications requiring the protection of delicate components by a soft solid, etc.

Acknowledgments

Financial support from the National Science Foundation (DMR 05-49353 and ECS 01-03307) is gratefully acknowledged.

References

[1] Matyjaszewski K. Macromolecular engineering: from rational design through precise macromolecular synthesis and processing to targeted macroscopic material properties. Prog Polym Sci 2005;30:858–75.
[2] Chiefari J, Chong YKB, Ercole F, Krstina J, Jeffery J, Le TPT, et al. RAFT1. Macromolecules 1998;31:5559.
[3] Wang J-S, Matyjaszewski K. Controlled/"living" radical polymerization. Atom transfer radical polymerization in the presence of transition-metal complexes. J Am Chem Soc 1995;117:5614–5.
[4] Goto A, Fukuda T. Kinetics of living radical polymerization. Prog Polym Sci 2004;29:329–85.
[5] Davis KA, Matyjaszewski K. Statistical, gradient, block, and graft copolymers by controlled/living radical polymerizations. Adv Polym Sci 2002;159:2–166.
[6] Matyjaszewski K, Xia J. Atom transfer radical polymerization. Chem Rev 2001;101:2921–90.
[7] Zhang M, Mueller AHE. Cylindrical polymer brushes. J Polym Sci Part A Polym Chem 2005;43:3461–81.
[8] Beers KL, Gaynor SG, Matyjaszewski K, Sheiko SS, Moeller M. The synthesis of densely grafted copolymers by atom transfer radical polymerization. Macromolecules 1998;31:9413–5.
[9] Matyjaszewski K, Qin S, Boyce JR, Shirvanyants D, Sheiko SS. Effect of initiation conditions on the uniformity of three-arm star molecular brushes. Macromolecules 2003;36:1843–9.
[10] Qin S, Matyjaszewski K, Xu H, Sheiko SS. Synthesis and visualization of densely grafted molecular brushes with crystallizable poly(octadecyl methacrylate) block segments. Macromolecules 2003;36:605–12.
[11] Qin S, Saget J, Pyun J, Jia S, Kowalewski T, Matyjaszewski K. Synthesis of block, statistical, and gradient copolymers from octadecyl

(meth)acrylates using atom transfer radical polymerization. Macromolecules 2003;36:8969–77.
[12] Neugebauer D, Zhang Y, Pakula T, Sheiko SS, Matyjaszewski K. Densely-grafted and double-grafted PEO brushes via ATRP. A route to soft elastomers. Macromolecules 2003;36:6746–55.
[13] Berry GC. Polymer rheology: principles, techniques and applications. In: Brady Jr RF, editor. Comprehensive desk reference of polymer characterization and analysis. Oxford: Oxford University Press; 2003. p. 574–623.
[14] Berry GC, Plazek DJ. Rheology of polymeric fluids. In: Uhlmann DR, Kreidl NJ, editors. Glass: science and technology viscosity and relaxation, vol. 3. London: Academic Press; 1986. p. 319–62.
[15] Ferry JD. Viscoelastic properties of polymers. New York: John Wiley & Sons Inc; 1979. p. 671.
[16] Graessley WW. Polymeric liquids and networks: structure and properties. New York: Garland Science; 2004. p. 559.
[17] de Gennes PG. Scaling concepts in polymer physics. Ithaca: Cornell University; 1979.
[18] Flory PJ. Principles of polymer chemistry. Ithaca: Cornell University Press; 1953.
[19] Pakula T, Matyjaszewski K. Polymers, supersoft elastomers and methods for preparing the same. PCT Int Appl 2004;65.
[20] Zhang Y, Okrasa L, Qin S, Lee H-i, Matyjaszewski K, Pakula T. Structure and mechanical properties of new low modulus elastomers. PMSE Prepr Am Chem Soc 2005;92:618–9.
[21] Tsukahara Y, Namba S-i, Iwasa J, Nakano Y, Kaeriyama K, Takahashi M. Bulk properties of poly(macromonomer)s of increased backbone and branch lengths. Macromolecules 2001;34:2624–9.
[22] Beers KL, Boo S, Gaynor SG, Matyjaszewski K. Atom transfer radical polymerization of 2-hydroxyethyl methacrylate. Macromolecules 1999; 32:5772–6.
[23] Qin S, Borner HG, Matyjaszewski K, Sheiko SS. Densely grafted molecular brushes with high molecular weight backbone by ATRP and RAFT techniques. Polym Prepr Am Chem Soc 2002;43(2):237–8.
[24] Boerner HG, Beers K, Matyjaszewski K, Sheiko SS, Moeller M. Synthesis of molecular brushes with block copolymer side chains using atom transfer radical polymerization. Macromolecules 2001;34: 4375–83.
[25] Matyjaszewski K, Patten TE, Xia J. Controlled/''living'' radical polymerization. Kinetics of the homogeneous atom transfer radical polymerization of styrene. J Am Chem Soc 1997;119:674–80.
[26] Sumerlin BS, Neugebauer D, Matyjaszewski K. Initiation efficiency in the synthesis of molecular brushes by grafting from via atom transfer radical polymerization. Macromolecules 2005;38:702–8.
[27] Berry GC. Molecular weight distribution. In: Bever MB, editor. Encyclopedia of materials science and engineering. Oxford: Pergamon Press; 1986. p. 3759.
[28] Sheiko SS, da Silva M, Shirvaniants D, LaRue I, Prokhorova S, Moeller M, et al. Measuring molecular weight by atomic force microscopy. J Am Chem Soc 2003;125:6725–8.
[29] Pakula T, Geyder S, Edling T, Boese D. Relaxation and viscoelastic properties of complex polymer systems. Rheol Acta 1996;35:631–44.
[30] Wu W, Huang J, Jia S, Kowalewski T, Matyjaszewski K, Pakula T, et al. Self-assembly of pODMA-*b*-ptBA-*b*-pODMA triblock copolymers in bulk and on surfaces. A quantitative SAXS/AFM comparison. Langmuir 2005;21:9721–7.
[31] Zhang Y, Chung IS, Huang J, Matyjaszewski K, Pakula T. Structure and properties of poly(butyl acrylate-*block*-sulfone-*block*-butyl acrylate) triblock copolymers prepared by ATRP. Macromol Chem Phys 2005; 206:33–42.
[32] Tong JD, Jerome R. Synthesis of poly(methyl methacrylate)-*b*-poly(*n*-butyl acrylate)-*b*-poly(methyl methacrylate) triblocks and their potential as thermoplastic elastomers. Polymer 2000;41:2499–510.
[33] Roovers J, Graessley WW. Melt rheology of some model comb polystyrenes. Macromolecules 1981;14:766–73.
[34] Plazek DJ, Seoul C, Bero CA. Diluent effects on viscoelastic behavior. J Non-Cryst Solids 1991;131(Pt. 2):570–8.
[35] Orbon SJ, Plazek DJ. Recoverable compliance of a series of bimodal molecular-weight blends of polystyrene. J Polym Sci Part B Polym Phys 1979;17:1871–90.
[36] Kapnistos M, Vlassopoulos D, Roovers J, Leal LG. Linear rheology of architecturally complex macromolecules: comb polymers with linear backbones. Macromolecules 2005;38:7852–62.
[37] Sebastian JM, Graessley WW, Register RA. Steady-shear rheology of block copolymer melts and concentrated solutions: defect-mediated flow at low stresses in body-centered-cubic systems. J Rheol 2002;46:863–79.